

Jet Charge and Machine Learning

Katherine Fraser and Matthew D. Schwartz

Department of Physics, Harvard University, Cambridge, MA 02138, USA

Abstract

Modern machine learning techniques, such as convolutional, recurrent and recursive neural networks, have shown promise for jet substructure at the Large Hadron Collider. For example, they have demonstrated effectiveness at boosted top or W boson identification or for quark/gluon discrimination. We explore these methods for the purpose of classifying jets according to their electric charge. We find that neural networks that incorporate distance within the jet as an input can provide significant improvement in jet charge extraction over traditional methods. We find that both convolutional and recurrent networks are effective and both train faster than recursive networks. The advantages of using a fixed-size input representation (as with the CNN) or a smaller input representation (as with the RNN) suggest that both convolutional and recurrent networks will be essential to the future of modern machine learning at colliders.

1 Introduction

As the Large Hadron Collider, currently running at CERN, increases in luminosity, it becomes sensitive to signals of beyond-the-standard model physics with ever smaller cross sections. These signals, particularly if they involve hadronic final states known as jets, are often buried in enormous backgrounds, so any tools that help reduce those backgrounds will be invaluable. In addition, increased clarity on jet properties and substructure will constrain and test the Standard Model. Over the last decade or so there has been tremendous progress in understanding jets and measuring their properties, from finding boosted top quark or W -jets [1–4], to looking at jet substructure [5,6]. Recently, new methods from computer science involving modern machine learning are starting to be adapted to jet physics, with remarkable early progress [7–20]

In this paper, we consider how modern machine learning might help in measuring the electric charge of a jet. Doing so accurately would allow us to differentiate up-quark initiated jets ($Q = \frac{2}{3}$) from anti-up-quark ($Q = -\frac{2}{3}$), down-quark ($Q = -\frac{1}{3}$), anti-down quark ($Q = \frac{1}{3}$) and gluon-initiated jets ($Q = 0$). This is clearly an ambitious goal, but there is already evidence that relatively simple observables, such as the p_T -weighted jet charge

$$\mathcal{Q}_\kappa^i = \frac{1}{(p_T^{\text{jet}})^\kappa} \sum_{j \in \text{jet}} Q_j (p_T^j)^\kappa \quad (1)$$

can help. This observable, adapted from early work of Feynman and Field [21], was shown in [22,23] to have appealing theoretical properties, such as a calculable scale-dependence. Measurements of \mathcal{Q}_κ^i by both ATLAS and CMS [24–30] confirmed its utility and demonstrated that, on average, positive and negative electrically charged jets can be distinguished. Moreover, the scale-dependence predicted in [22,23] was confirmed experimentally [24]. Thus, considering that jet charge can already be measured to some extent, it is natural to ask if we can do better using deep learning or other modern machine-learning ideas.

The challenge of extracting the jet electric charge is not unlike the challenge of extracting the jet color charge, namely whether a jet is quark- or gluon initiated. Quark/gluon jet discrimination also has a long history [31–34]. Some Monte-Carlo studies showed good potential for the LHC [35,36], and experimental studies showing feasibility while also uncovering some challenges (such as the untrustworthiness of the simulations particularly for gluon jets) [37]. One of the first modern-machine-learning jet physics papers [8] showed that, using convolutional neural networks (CNNs) and jet images [38,39], demonstrated a significant improvement over previous quark-gluon discrimination benchmarks (see also [16,39–41]). Work on testing this method in experiment is ongoing [42].

While the jet images approach is powerful, it involves embedding the jet data in a very high dimensional representation. For example, a jet may have 50 particles, so it is characterized by 50 three-momenta, or 150 degrees of freedom. A 33×33 jet image has 1089 degrees of freedom. Alternatives to jet images are methods such as recursive and recurrent neural networks. Thus besides developing a powerful jet charge discriminator, one goal of this paper is to compare the performance of different network architectures on jet charge extraction and quark/gluon discrimination.

Recurrent neural networks have been considered for collider physics applications in [13, 17]. In particular [13] considered the application of a particular recurrent framework for top-tagging and found comparable performance to a jet-images based approach [16]. A challenge with recurrent networks is how to sort and process the inputs. One option is to use 4-vectors, as in [13, 17]. In [13] the 4-vectors were processed with a network constructed to respect their Lorentz structure. We will instead consider recurrent network inputs containing various distillations of the 4-vector input, such as into the energy or the jet, or the clustering distance to the jet axis.

The paper is divided into two parts: a discussion of the networks in Section 2 and a discussion of the results in Section 3. A summary and broader conclusions are in Section 4.

2 Methods

For this study, we simulated quark and gluon jets using PYTHIA 8.226 [43] with the default tune. For jet charge, we focused on discriminating up-quark-initiated jets from down-quark-initiated jets. These jets were selected as the hardest jet in $uu \rightarrow uu$ or $dd \rightarrow dd$ dijet events in pp collisions with $\sqrt{s} = 13$ TeV. For quark/gluon discrimination, the processes $pp \rightarrow qq$ and $pp \rightarrow gg$ were used and again the hardest jet taken. Jets were clustered with the anti- k_T algorithm with $R = 0.4$. Final state particles with $|\eta| > 2.5$ and neutrinos were discarded.

We consider a number of different machine learning methods.

2.1 Convolutional networks (jet images)

From each event we constructed a jet image, following the procedure of [8]. Images are constructed by putting a $\Delta\phi \times \Delta\eta = 33 \times 33$ pixel box around each jet. We considered two-channel jet images. For the first channel, the pixel intensity is given by the sum of the transverse momenta of all particles entering that pixel. For the second channel, the pixel intensity is given by the p_T -weighted jet charge, as in Eq. (1), for a given κ . During image generation, the image is centered and the momentum channel is normalized by the sum of the momenta. The same preprocessing and data augmentation as [8] was used on the images. This preprocessing includes zero centering and dividing by the standard deviation, and data augmentation includes translations by one pixel in each direction and reflections. A random rotation was tested but did not improve performance.

The images are processed with a convolutional neural network, as in [8]. Our basic CNN consisted of three 2-dimensional convolutional filters, one dense layer with 64 neurons, and a final dense layer with 2 neurons. Each convolutional layer is followed by a maxpooling layer and a dropout layer and the first dense layer is followed by a dropout layer. The dropout was 0.18 for the first layer and 0.35 for the other layers. The convolutional layers and the first dense layer have ReLU activations, while the second dense layer has a softmax activation. The network was trained in batches of 512 for 35 epochs with an early stopping patience of 5 epochs, using the Adam algorithm and categorical crossentropy loss function. Each layer

had 64 filters. The filter size was 8×8 pixels for the first layer and 4×4 pixels for the other layers.

Other network parameters were also tested. For two-channel images, we considered the effect of modifying the step size and decay within optimization, batch size, the dropout after each layer, filter size, number of filters, size of the maxpooling layer, activation function for the convolutional layers (selu), early stopping patience, and optimizer (SGD, RMS Prop, Adagrad). We also experimented with modifying network structure by adding additional convolutional layers at the beginning of the network and extra dense layers after the convolutional layers. The configuration detailed above was the most effective.

In addition to modifying network structure, we tried modifying the content of the channels of the network by adding a third channel with more information. Adding a third channel with the number of neutral particles did not improve results. Adding a third channel with jet charge per pixel for a second κ value did improve training speed, but not results (see Fig. 3a). Furthermore, with a second κ value the dropout value needed to be higher to avoid over training.

We also implemented the traditional multivariate method of boosted decision trees (BDTs) to combine p_T weighted jet charge with various κ values. Our implementation of BDTs is with scikitlearn using AdaBoostClassifier with 500 samples per leaf minimum, 10 estimators, and learning rate 0.5 (based on a scan of a selection of parameters).

Additionally, we tested a residual CNN, which uses shortcut connections that connect a given layer to some previous layers while skipping one or more intermediate layers. We model our network on [44], which won the ILSVRC 2015 image recognition challenge. In particular, we use the identity mapping as our shortcut connection, so that the output of each convolutional layer except the first is added to the input of that layer before it is passed to the next layer, which in [44] was shown to improve classification in previous image recognition challenges. Following the observation in [44] that residual CNNs show more improvement for deeper networks, we use a deeper network than our other CNN. We use seven layers each with 64 filters of size 2×2 . We use smaller filters than our other CNN because of memory constraints for the deeper network. There is a maxpooling layer of size 4 after the fourth and eighth layers, and a maxpooling layer with size two after the seventh layer. As with the shallower CNN, the convolutional layers are immediately followed by two dense layers, the first with 64 nodes and the second with 2 nodes. Dropout of 0.2 was used after each maxpooling layer, and dropout of 0.1 was used after the first dense layer. These parameters were determined by a scan of selection of parameters. Other hyperparameters are the same as in the shallower network.

2.2 Recurrent networks

We also tested a recurrent network with various different inputs. In a recurrent network, each layer consists of multiple nodes, each with a set of hidden weights. Both the input and output of each layer is an ordered sequence of vectors, where each vector in the sequence has fixed length but the length of the sequence itself is arbitrary. The length of each output vector is the same as the number of nodes, and the length of the output sequence is the same

as the length of the input sequence. Network performance is very sensitive to the order of the input vectors.

We implemented a recurrent network using keras [45] with a Theano backend. It consists of 11 gated recurrent unit layers (GRUs), followed by a dense layer with 64 nodes and a dense layer with two output nodes. The number of nodes in each GRU layer decreases from 100 to 5, where the number of nodes in each of the first ten layers decreases by ten from the previous layer. Each GRU layer except the last returns a sequence of vectors, and the last returns the average of the sequence of vectors. The number and size of the GRU layers were determined by trial and error. An additional dense layer of 64 units was tested but decreased classification effectiveness. Long short-term memory (LSTM) layers were also tested and performed similarly to GRU layers. Additionally, we tested various different input representations. We considered combinations of azimuthal angle ϕ , pseudorapidity η , p_T , charge Q and various distance measures.

A batch size of 6000 was used for training with step size of 0.005. Other batch sizes were tested. We found that for small batch sizes training was very slow and non-convergent. Training improved with larger batch size up to 6000. A step size of 0.001 was also tested but training was more consistent with a smaller step size. Optimization was performed using the Adam algorithm with a categorical cross entropy loss function and early stopping patience of 3 and a maximum of 100 epochs. In order to use keras a maximum sequence length must be set for the input layer. We set this to 40 particles for 100 GeV and 120 particles for 1000 GeV, so that it would include enough particles not to affect training.

A last dense layer with a single output node attempting to predict charge itself (instead of classification) was also tested. Here mean squared error was used as the loss function, as categorical cross entropy only makes sense for classification. In this case we tested a linear activation function (instead of a ReLU) for the second of the two dense layers, because we wanted to be able to predict negative values. This network performed similarly to classification.

In addition, a dense network with similar parameters that used the hardest N particles as input was also tested, with N ranging from 5 to 10, with 8 particles appearing optimal. This did not even perform as well as p_T -weighted jet charge alone. A variety of filter configurations were tested for this network.

2.3 Recursive network

A recursive network is a generalization of a recurrent network. In a recurrent network, the same set of weights is applied to every vector in an ordered sequence of vectors. For a given node in a recurrent network, each computation depends directly only on the input vector to that step and the internal hidden state after the previous step in the sequence. Recursive networks can have more complicated dependency structures than an ordered sequence. Rather than applying the same set of weights to every vector in a sequence, a recursive network applies the same weights in an order given by a more complicated data structure, such as a tree. In any given step, the input to a recursive node can be an encoding of leaves in the tree, an encoding of interior nodes in the tree, or a combination of both.

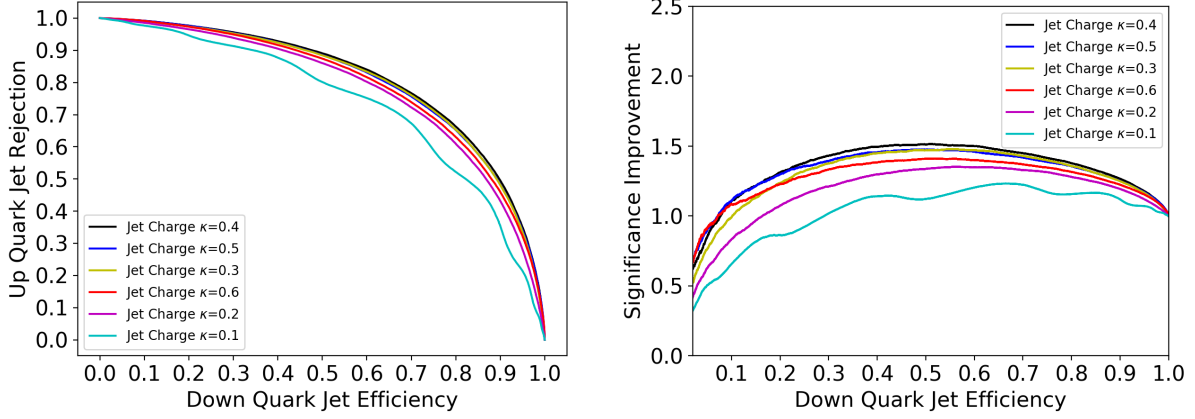


Figure 1: ROC and SIC curves for p_T -weighted jet charge for various κ .

The architecture of our recursive network is modeled after [17]. A recursive embedding, given by Eqs. (2) through (4) of [17], with $v_{i(k)}$ consisting of p_T, ϕ, η and charge Q , is fed into a classifier consisting of a dense layer with 64 nodes followed by a dense layer of 2 nodes. The recursive embedding consists of a single vector given by the embedding at the root node. Clustering is performed prior to passing the information to the network following the C/A, anti- k_T , and k_T algorithms (in all cases, our jets are the same collection of particles identified with anti- k_T). For leaf nodes the charge Q is the charge of the particle corresponding to the leaf. For interior nodes, the charge Q is taken to be the p_T -weighted jet charges of the left and right children with $\kappa = 0.2$ at 100 GeV and $\kappa = 0.1$ at 1000 GeV.

We also tested a simpler recursive structure inspired by jet charge. The first half of this network is recursively computed jet charge with trainable κ values, while the second half is a dense layer with two nodes. Which κ to use to compute the value at each node is determined by the distance from the root node in the clustering tree. For the plots in this paper, we used five κ values, and the recursively computed jet charge of all nodes with distance greater than or equal to five from the root node were computed using the last κ . The other hyperparameters for this network were similar to those for the other recursive network.

3 Results

In this section we present our results. The figures below include displays of the standard Receiver-Operator Characteristic (ROC) curve of the down-quark (signal) efficiency ϵ_s versus up-quark (background) efficiency ϵ_b and of the Significance Improvement Characteristic (SIC) curve of $\epsilon_s/\sqrt{\epsilon_b}$ [46]. The SIC curves indicate approximately the improvement on discrimination significance and their peak values, $\overline{\text{SIC}}$ gives an objective uniform quantitative measure of performance. ROC curves and SIC curves convey the same information.

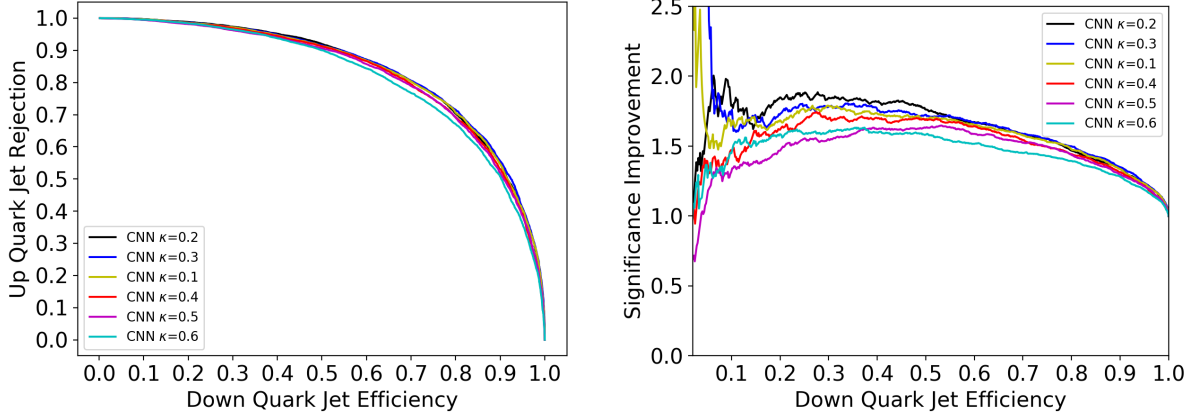


Figure 2: ROC and SIC curves for jet-image based CNNs using two input images: the total p_T and the p_T -weighted jet charge, for various κ as listed.

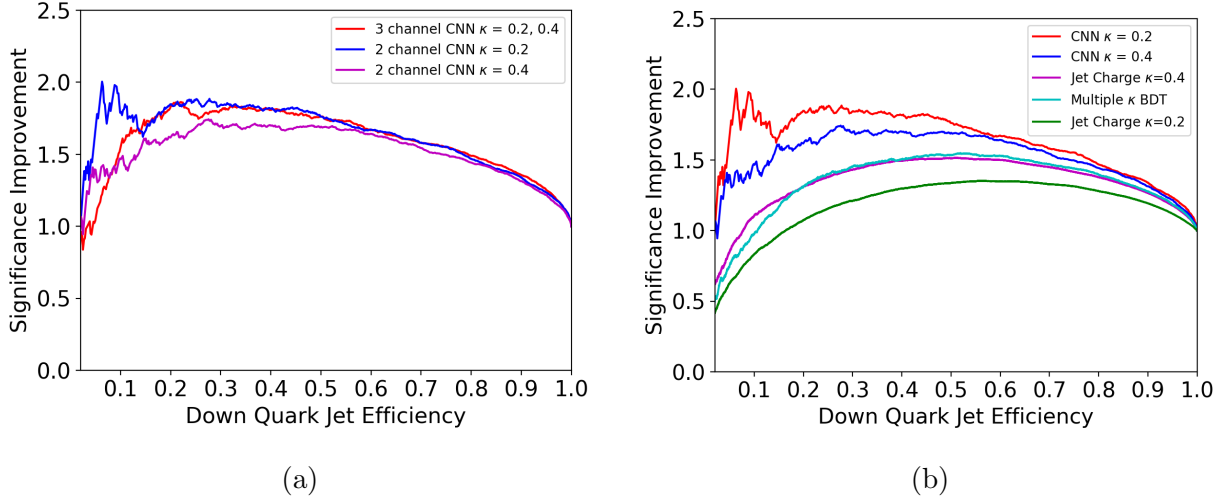


Figure 3: (a) Comparison of 2 and 3-input channel CNNs. Two κ values are used for the 3 channel images, in addition to the total momentum input channel. (b) Comparison of p_T -weighted jet charge, CNNs using two-channel jet images, and a BDT of multiple jet charges.

3.1 p_T -weighted jet charge

We first evaluate the effectiveness of the p_T -weighted jet charge in Eq. (1) for various values of κ . The result is shown in Fig. 1. These results are consistent with those in [22], showing optimal performance at $\kappa = 0.4$ with $\overline{\text{SIC}} = 1.5$.

3.2 Jet Images

Next, we look at the performance of our CNN using 2-channel jet images on the same samples. The results are shown in Fig. 2 for various κ values. We see that the optimal κ value for jet images is $\kappa = 0.2$, which is lower than for p_T -weighted jet charge. The performance of the CNN is also better with $\overline{\text{SIC}} = 1.8$, a notable improvement.

Fig. 3a compares the performance of the CNN with two input layers (one value of κ) to a CNN with 3 input layers, with the 3rd layer being the p_T -weighted jet charge with a different value of κ . We see that adding the extra layer does not improve performance.

Fig. 3b compares the traditional p_T -weighted jet charge to the two-channel CNN with $\kappa = 0.2$ and to the two-channel CNN with $\kappa = 0.4$. Included in these plots are a curve using a BDT constructed by combining the p_T -weighted jet charge with $\kappa = 0.2, 0.3$ and 0.4 . We see that the CNN outperforms both the single κ observable and the multiple κ value BDT.

3.3 Recurrent Network Results

Next we explore the performance of a recurrent neural network with a variety of different input vectors associated to each input momentum. We considered combinations of azimuthal angle ϕ , pseudorapidity η , p_T , charge Q and various distance measures. The configurations we tried were

1. (η, ϕ, p_T, Q)
2. $(\eta, \phi, p_T, Q, d_1, \dots, d_n)$ where the d_i are the distances to the hardest N anti- k_T subjects using C/A , k_T , or anti- k_T distance measures
3. (η, ϕ, p_T, Q, d) where d is the clustering-tree distance to root node
4. (η, ϕ, p_T, Q, d) where d is the distance to the jet axis using C/A , k_T , or anti- k_T distance measures
5. (p_x, p_y, p_z, E, Q)

A comparison of the different RNN inputs is displayed in Fig. 4a. All networks that take distance as input in Fig. 4a use the C/A distance. All configurations discussed above show slight improvement over jet charge. Configurations 1 and 5 perform only slightly better than jet charge, while the other RNNs perform noticeably better. We believe this is because configurations 2 through 4 all incorporate a measure of distance within the jet, similar to the CNN and RecNN displayed in Fig. 6.

Performance of configuration 4 for the different distance measures is explored further in Fig. 4b. For configuration 2 the best performance was achieved for $N = 2$ with a subjet radius of 0.001 and step size of 0.003.

We find that at low energy reading the input data and training is noticeably faster with the recurrent network than with jet images. Additionally, the training and performance of the recurrent network is sensitive to the ordering of the inputs and does not train unless they

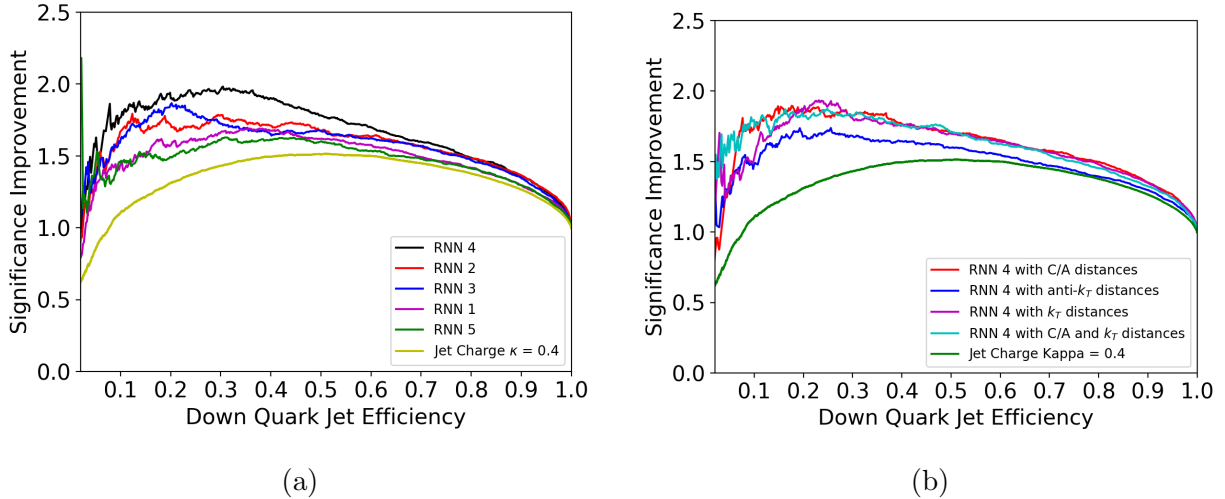


Figure 4: (a) Comparison of different RNN inputs to jet charge. Configuration 2 uses $N = 2$. Configurations which include distance to the jet axis or hardest particles perform better than those that do not. (b) Performance of recurrent neural networks in configuration 4 using p_T , charge Q and distance to jet axis as inputs.

are sorted. For the plots displayed in this paper, inputs are sorted in order of decreasing p_T , but we found that sorting by increasing distance from the jet axis is equally effective. We also found that including other extra information, in addition to the inputs of configuration 1, inhibit training, sometimes to the point where the network is unable to reach an acceptance better than fifty percent. This suggests that including extra information in the RNN can actually hurt its performance. Various normalization configurations were tested, including zero centering and dividing by the standard deviation for a single jet, and zero centering and normalizing all channels across jets. Normalizing only the p_T channel across jets was the only configuration that performed better than the raw vectors at 100 GeV. At 1000 GeV, this normalization was required to achieve an acceptance of better than fifty percent.

3.4 Recursive Network Results

The recursive network (RecNN) performed slightly worse than both the CNN and RNN, and also took much longer to train. However, the RecNN (like the CNN) can train with a small training set (16,000 events instead of 160,000), while the RNN does not achieve an acceptance of better than fifty percent for such a small training set.

A comparison of the top performing convolutional, recurrent and recursive networks is shown in Fig. 6. The area-under-the-ROC-curve (AUC) metric and the up quark efficiency at 50% down quark efficiency are displayed in Table 1.

Network	100 GeV		1000 GeV	
	Up Quark Efficiency	AUC	Up Quark Efficiency	AUC
RecNN	0.085	0.834	0.049	0.876
CNN	0.080	0.837	0.048	0.879
RNN	0.079	0.841	0.054	0.874
Residual CNN	0.078	0.840	0.053	0.877
Multiple κ	0.104	0.815	0.080	0.841
Jet Charge	0.109	0.810	0.090	0.832

Table 1: Up quark efficiency at 50% down quark efficiency and area-under-the-ROC-curve (AUC) at 100 and 1000 GeV. Jet charge has $\kappa = 0.4$ at 100 GeV and $\kappa = 0.3$ at 1000 GeV. All NNs except the multiple κ network noticeably outperform p_T weighted jet charge. In the 100 GeV case, both CNNs and the RNN perform about equally well while the RecNN performs slightly worse. In the 1000 GeV case, the CNNs and RecNN give the best results, while the RNN performs slightly worse.

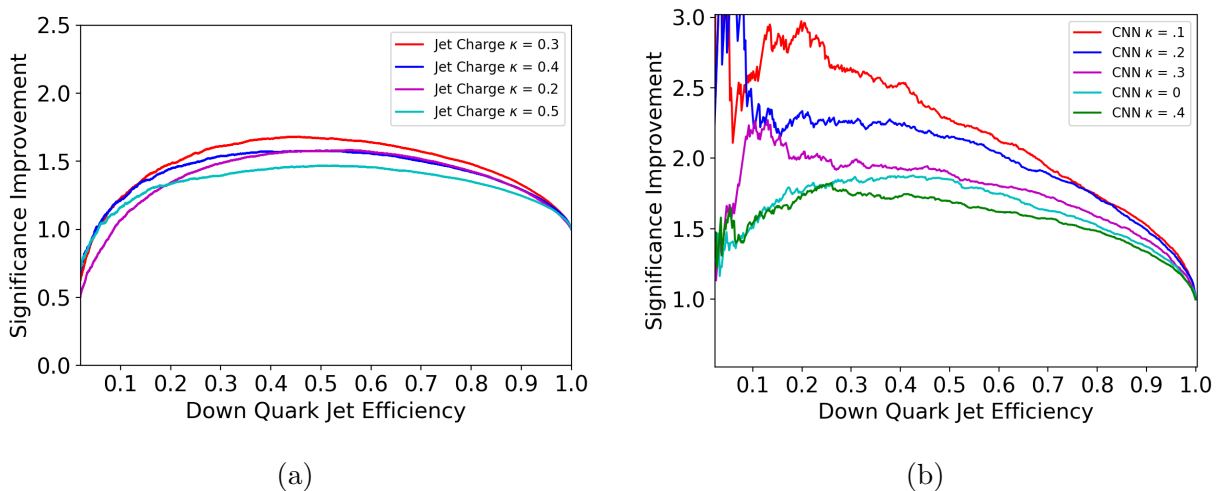


Figure 5: (a) Comparison of jet charge for various κ values at 1000 GeV. (b) Comparison of CNN performance for various κ values at 1000 GeV.

3.5 Energy Dependence

The results discussed above were all based on 100 GeV jets. The analysis was repeated for 1000 GeV jets. More precisely, up and down quark events were regenerated with p_T between 1000 GeV and 1200 GeV, with all other parameters being the same. We found discrimination power improves for all methods at higher p_T . This is of course expected and consistent with previous results [22–24]. Results are shown in Fig. 7. There was improvement in all methods, but the relative improvement of the RNN, CNN and RecNN over the p_T -weighted jet charge is larger at 1000 GeV than at 100 GeV. We also see that at 1000 GeV the RecNN and CNNs

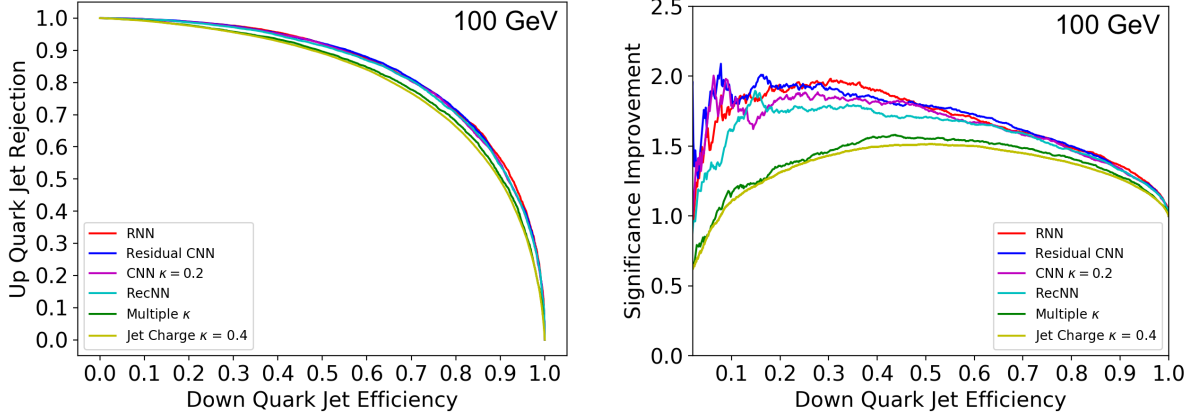


Figure 6: Comparison of the p_T -weighted jet charge to the best performing recurrent (RNN), recursive (RecNN), convolutional (CNN) neural networks for 100 GeV jets. The CNN is a two-input layer CNN with $\kappa = 0.2$. The RNN is of type 4 using the C/A distance. Both CNNs and the RNN perform noticeably outperform the p_T weighted jet charge. The RecNN performs slightly worse than the RNN and CNNs, while the multiple κ network only slightly outperforms jet charge.

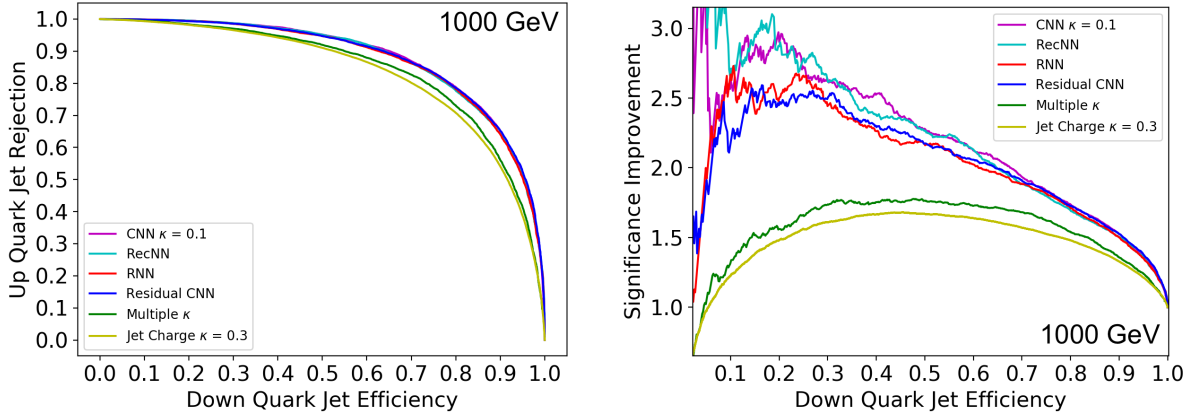


Figure 7: Comparison of best performing recurrent (RNN), recursive (RecNN), convolutional (CNN) neural networks with p_T -weighted jet charge at 1000 GeV. The improvement between the RNN, CNN or the RecNN and jet charge was larger than in the 100 GeV case.

perform better than the RNN, in contrast to at 100 GeV where the RNN was best.

Figs. 5a and 5b try different values of κ for the p_T weighted jet charge and for the two-input-layer CNN. We see that the optimal κ for both jet charge and the CNN decreases with energy. At 1000 GeV, the optimal κ for the CNN is still smaller than the optimal κ for jet charge.

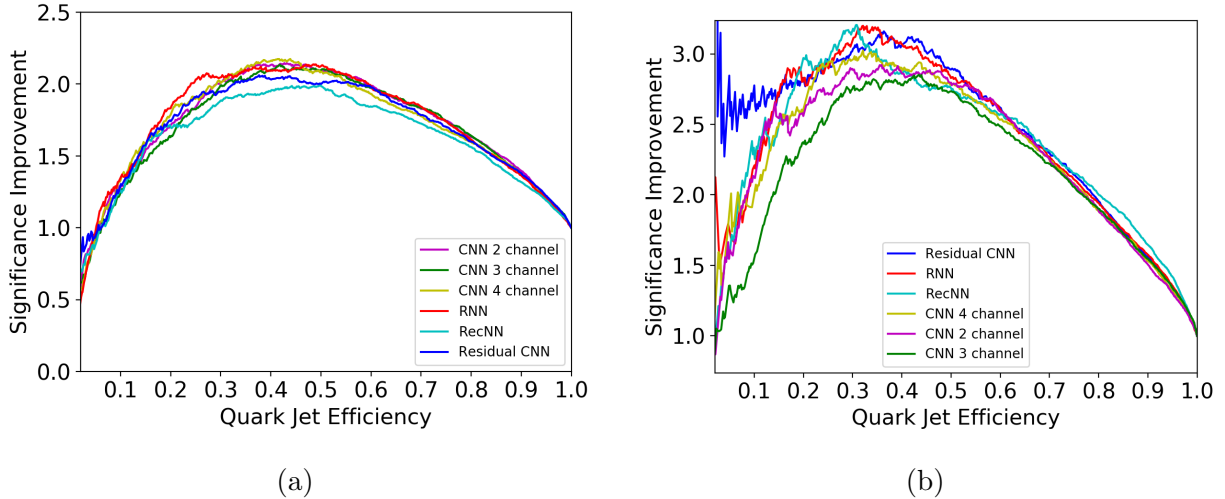


Figure 8: (a) Comparison of various network architectures for quark/gluon discrimination at 100 GeV. (b) Comparison of various network architectures for quark/gluon discrimination at 1000 GeV.

3.6 Quark/Gluon discrimination

Finally, we examine how the network architectures that we have used for jet charge work for quark/gluon discrimination. We compare our networks to each other as well as to the three-channel images used in [8], where one channel is total p_T , one is charged particle p_T and the third is particle multiplicity. For completeness, we also consider four-channel images with three channels as in [8] and a fourth having p_T -weighted jet charge with $\kappa = 0.2$ at 100 GeV and $\kappa = 0.1$ at 1000 GeV (the same values as the best performing κ in the up versus down quark case). We look at both 100 GeV and 1000 GeV jets.

Fig. 8a is a comparison plot of the different methods. We see that most methods have comparable performance, with the exception of the recursive neural network that performs worse. At 1000 GeV, the comparison is shown in Fig. 8b. We find in this case that the recurrent network does noticeably better than the jet images network.

4 Conclusions

In this paper we have applied techniques of modern machine learning to the problem of measuring the electric charge of a jet. In particular, we have used these networks to discriminate jets initiated by up-quarks (charge $Q = \frac{2}{3}$) from those initiated by down-quarks (charge $Q = -\frac{1}{3}$). The reference discriminator is the p_T -weighted jet charge [22] which has optimal performance for $\kappa \approx 0.4$ at 100 GeV and optimal performance for $\kappa \approx 0.3$ at 1000 GeV. The network architectures we considered include convolutional, residual convolutional, recurrent and recursive networks.

The CNNs are used to process jet images, with 2, 3 or 4 “colors” (input layers) modeled

after the quark/gluon study in [8]. We find these CNNs perform significantly better than the p_T -weighted jet charge. We also studied residual CNNs, but they did not improve performance compared to our other CNNs. For the recurrent networks we considered a variety of different inputs. Recurrent networks take as input a list of variables associated with each particle, such as the 4-momenta or charge. We tried a number of different input sets and found that taking p_T , charge Q , and the C/A clustering distance to the jet axis works the best. We also studied a recursive network with multiple trainable κ 's, but this network barely outperformed jet charge. With the exception of this last network, all of our networks noticeably perform better than p_T -weighted jet charge.

There are a few general lessons we have learned about networks from this study. At high signal efficiency, all the networks that explicitly incorporate distances from within the jet or from the jet's clustering history perform about equally well. At low signal efficiency, which network performs best is dependent on both the type of jets and the jet's energy. We found that tuning hyperparameters and normalization conventions has similar effects on performance for all networks. This suggests that while it is important to customize the size and parameters of a network to the specific application, in the case of up versus down jet identification any network that encodes distances effectively should perform close to optimal. We see similar results in the quark gluon case. Since the networks perform equivalently, the difficulty of training the network should be an important consideration. An advantage of the CNN architecture is that it requires less modification with energy scale because the input representation size is fixed. An advantage of the RNN is that the input size is smaller which noticeably improves training time over the CNN, particularly at low energies. Training the RecNN is generally slow. Thus we find both the CNN and RNN to be more promising than the RecNN.

Our best networks can distinguish up and down quark jets significantly better than previous methods. At a 50% down-quark efficiency working point, the networks allow us to reject all but 8% of up-quark jets at 100 GeV (with a CNN or RNN) and all but 5% of up-quark jets at 1000 GeV (with a CNN or a RecNN). This rejection rates improve on previous methods by almost a factor of 2 at high energy.

In conclusion, we have shown that machine learning can produce significant improvement in distinguishing up and down quark jets over traditional approaches. Our summary plots of in Figs. 6 and 7. Neural networks that explicitly incorporate distance are the most effective. Both convolutional networks, like those used in [8], and recurrent neural networks perform very well. The performance of the recurrent network depends on its inputs: we find it is important to reduce the inputs from the raw 4-vectors to the energy and some distance measure. In principle, the network should learn this reduction, but doing so may require a very large network or enormously long training times. By processing the RNN inputs in this way, training is much faster and performance better.

Although our networks work well, it is clear that there is still room for improvement. We expect that jet charge will continue to serve both as a valuable phenomenological tool and as a benchmark challenge for machine learning methods for the foreseeable future.

Acknowledgements

The authors would like to thank B. Nachman and J. Andreas for discussions. MDS is supported in part by the Department of Energy under contract DE-SC0013607. Support for KF was provided in part by the Harvard Data Science Initiative. The computations in this paper were run on the Odyssey cluster supported by the FAS Division of Science, Research Computing Group at Harvard University.

References

- [1] D. E. Kaplan, K. Rehermann, M. D. Schwartz, and B. Tweedie, “Top Tagging: A Method for Identifying Boosted Hadronically Decaying Top Quarks,” *Phys. Rev. Lett.* **101** (2008) 142001, [arXiv:0806.0848 \[hep-ph\]](#).
- [2] L. G. Almeida, S. J. Lee, G. Perez, G. F. Sterman, I. Sung, and J. Virzi, “Substructure of high-pT Jets at the LHC,” *Phys. Rev.* **D79** (2009) 074017, [arXiv:0807.0234 \[hep-ph\]](#).
- [3] Y. Cui, Z. Han, and M. D. Schwartz, “W-jet Tagging: Optimizing the Identification of Boosted Hadronically-Decaying W Bosons,” *Phys. Rev.* **D83** (2011) 074023, [arXiv:1012.2077 \[hep-ph\]](#).
- [4] J. Thaler and K. Van Tilburg, “Maximizing Boosted Top Identification by Minimizing N-subjettiness,” *JHEP* **02** (2012) 093, [arXiv:1108.2701 \[hep-ph\]](#).
- [5] G. P. Salam, “Towards Jetography,” *Eur. Phys. J.* **C67** (2010) 637–686, [arXiv:0906.1833 \[hep-ph\]](#).
- [6] A. Altheimer *et al.*, “Jet Substructure at the Tevatron and LHC: New results, new tools, new benchmarks,” *J. Phys.* **G39** (2012) 063001, [arXiv:1201.0008 \[hep-ph\]](#).
- [7] L. de Oliveira, M. Kagan, L. Mackey, B. Nachman, and A. Schwartzman, “Jet-images ? deep learning edition,” *JHEP* **07** (2016) 069, [arXiv:1511.05190 \[hep-ph\]](#).
- [8] P. T. Komiske, E. M. Metodiev, and M. D. Schwartz, “Deep learning in color: towards automated quark/gluon jet discrimination,” *JHEP* **01** (2017) 110, [arXiv:1612.01551 \[hep-ph\]](#).
- [9] P. T. Komiske, E. M. Metodiev, B. Nachman, and M. D. Schwartz, “Pileup Mitigation with Machine Learning (PUMML),” *JHEP* **12** (2017) 051, [arXiv:1707.08600 \[hep-ph\]](#).
- [10] H. Luo, M.-x. Luo, K. Wang, T. Xu, and G. Zhu, “Quark jet versus gluon jet: deep neural networks with high-level features,” [arXiv:1712.03634 \[hep-ph\]](#).

- [11] T. Cheng, “Recursive Neural Networks in Quark/Gluon Tagging,” [arXiv:1711.02633 \[hep-ph\]](#).
- [12] E. M. Metodiev, B. Nachman, and J. Thaler, “Classification without labels: Learning from mixed samples in high energy physics,” *JHEP* **10** (2017) 174, [arXiv:1708.02949 \[hep-ph\]](#).
- [13] A. Butter, G. Kasieczka, T. Plehn, and M. Russell, “Deep-learned Top Tagging using Lorentz Invariance and Nothing Else,” [arXiv:1707.08966 \[hep-ph\]](#).
- [14] T. Cohen, M. Freytsis, and B. Ostdiek, “(Machine) Learning to Do More with Less,” [arXiv:1706.09451 \[hep-ph\]](#).
- [15] J. Pearkes, W. Fedorko, A. Lister, and C. Gay, “Jet Constituents for Deep Neural Network Based Top Quark Tagging,” [arXiv:1704.02124 \[hep-ex\]](#).
- [16] G. Kasieczka, T. Plehn, M. Russell, and T. Schell, “Deep-learning Top Taggers or The End of QCD?,” *JHEP* **05** (2017) 006, [arXiv:1701.08784 \[hep-ph\]](#).
- [17] G. Louppe, K. Cho, C. Becot, and K. Cranmer, “QCD-Aware Recursive Neural Networks for Jet Physics,” [arXiv:1702.00748 \[hep-ph\]](#).
- [18] A. J. Larkoski, I. Mould, and B. Nachman, “Jet Substructure at the Large Hadron Collider: A Review of Recent Advances in Theory and Machine Learning,” [arXiv:1709.04464 \[hep-ph\]](#).
- [19] P. T. Komiske, E. M. Metodiev, B. Nachman, and M. D. Schwartz, “Learning to Classify from Impure Samples,” [arXiv:1801.10158 \[hep-ph\]](#).
- [20] S. Macaluso and D. Shih, “Pulling Out All the Tops with Computer Vision and Deep Learning,” [arXiv:1803.00107 \[hep-ph\]](#).
- [21] R. D. Field and R. P. Feynman, “A Parametrization of the Properties of Quark Jets,” *Nucl. Phys.* **B136** (1978) 1.
- [22] D. Krohn, M. D. Schwartz, T. Lin, and W. J. Waalewijn, “Jet Charge at the LHC,” *Phys. Rev. Lett.* **110** no. 21, (2013) 212001, [arXiv:1209.2421 \[hep-ph\]](#).
- [23] W. J. Waalewijn, “Calculating the Charge of a Jet,” *Phys. Rev.* **D86** (2012) 094030, [arXiv:1209.3019 \[hep-ph\]](#).
- [24] **ATLAS** Collaboration, T. A. collaboration, “Jet Charge Studies with the ATLAS Detector Using $\sqrt{s} = 8$ TeV Proton-Proton Collision Data,”.
- [25] **ATLAS** Collaboration, B. Nachman, “Jet Charge with the ATLAS Detector using $\sqrt{s} = 8$ TeV pp Collision Data,” in *Proceedings, 2nd Conference on Large Hadron Collider Physics Conference (LHCP 2014): New York, USA, June 2-7, 2014*. 2014.

- [arXiv:1409.0318 \[hep-ex\]](https://arxiv.org/abs/1409.0318).
<https://inspirehep.net/record/1313120/files/arXiv:1409.0318.pdf>.
- [26] T. A. collaboration, “Measurement of jet charge in dijet events from $\sqrt{s} = 8$ TeV pp collisions with the ATLAS detector,”.
- [27] **ATLAS** Collaboration, G. Aad *et al.*, “Measurement of jet charge in dijet events from $\sqrt{s}=8$ TeV pp collisions with the ATLAS detector,” *Phys. Rev.* **D93** no. 5, (2016) 052003, [arXiv:1509.05190 \[hep-ex\]](https://arxiv.org/abs/1509.05190).
- [28] **CMS** Collaboration, C. Collaboration, “Measurement of jet charge observables in dijet events at $\sqrt{s} = 8$ TeV,”.
- [29] **CMS** Collaboration, A. M. Sirunyan *et al.*, “Measurements of jet charge with dijet events in pp collisions at $\sqrt{s} = 8$ TeV,” *JHEP* **10** (2017) 131, [arXiv:1706.05868 \[hep-ex\]](https://arxiv.org/abs/1706.05868).
- [30] **ATLAS, CMS** Collaboration, S. Tokar, “Jet charge determination at the LHC,” in *Proceedings, Parton Radiation and Fragmentation from LHC to FCC-ee: CERN, Geneva, Switzerland, November 22-23, 2016*, pp. 79–84. 2017.
https://inspirehep.net/record/1512998/files/1512294_79-84.pdf.
- [31] J. Pumplin, “How to tell quark jets from gluon jets,” *Phys. Rev.* **D44** (1991) 2025–2032.
- [32] L. Lonnblad, C. Peterson, and T. Rognvaldsson, “Finding Gluon Jets With a Neural Trigger,” *Phys. Rev. Lett.* **65** (1990) 1321–1324.
- [33] **OPAL** Collaboration, P. D. Acton *et al.*, “A Study of differences between quark and gluon jets using vertex tagging of quark jets,” *Z. Phys.* **C58** (1993) 387–404.
- [34] **OPAL** Collaboration, G. Alexander *et al.*, “A Direct observation of quark - gluon jet differences at LEP,” *Phys. Lett.* **B265** (1991) 462–474.
- [35] J. Gallicchio and M. D. Schwartz, “Quark and Gluon Jet Substructure,” *JHEP* **04** (2013) 090, [arXiv:1211.7038 \[hep-ph\]](https://arxiv.org/abs/1211.7038).
- [36] J. Gallicchio and M. D. Schwartz, “Quark and Gluon Tagging at the LHC,” *Phys. Rev. Lett.* **107** (2011) 172001, [arXiv:1106.3076 \[hep-ph\]](https://arxiv.org/abs/1106.3076).
- [37] **ATLAS** Collaboration, G. Aad *et al.*, “Light-quark and gluon jet discrimination in pp collisions at $\sqrt{s} = 7$ TeV with the ATLAS detector,” *Eur. Phys. J.* **C74** no. 8, (2014) 3023, [arXiv:1405.6583 \[hep-ex\]](https://arxiv.org/abs/1405.6583).
- [38] J. Cogan, M. Kagan, E. Strauss, and A. Schwartzman, “Jet-Images: Computer Vision Inspired Techniques for Jet Tagging,” *JHEP* **02** (2015) 118, [arXiv:1407.5675 \[hep-ph\]](https://arxiv.org/abs/1407.5675).

- [39] L. G. Almeida, M. Backovi, M. Cliche, S. J. Lee, and M. Perelstein, “Playing Tag with ANN: Boosted Top Identification with Pattern Recognition,” *JHEP* **07** (2015) 086, [arXiv:1501.05968 \[hep-ph\]](#).
- [40] P. Baldi, K. Bauer, P. Eng, Clara and Sadowski, and D. Whiteson, “Jet Substructure Classification in High-Energy Physics with Deep Neural Networks,” *Phys. Rev.* **D93** no. 9, (2016) 094034, [arXiv:1603.09349 \[hep-ex\]](#).
- [41] D. Guest, J. Collado, P. Baldi, S.-C. Hsu, G. Urban, and D. Whiteson, “Jet Flavor Classification in High-Energy Physics with Deep Neural Networks,” *Phys. Rev.* **D94** no. 11, (2016) 112002, [arXiv:1607.08633 \[hep-ex\]](#).
- [42] **ATLAS Collaboration** Collaboration, “Quark versus Gluon Jet Tagging Using Jet Images with the ATLAS Detector,” Tech. Rep. ATL-PHYS-PUB-2017-017, CERN, Geneva, Jul, 2017. <http://cds.cern.ch/record/2275641>.
- [43] T. Sjostrand, S. Mrenna, and P. Z. Skands, “A Brief Introduction to PYTHIA 8.1,” *Comput. Phys. Commun.* **178** (2008) 852–867, [arXiv:0710.3820 \[hep-ph\]](#).
- [44] K. He, X. Zhang, S. Ren, and J. Sun, “Deep Residual Learning for Image Recognition,” [arXiv:1512.03385 \[cs.CV\]](#).
- [45] F. Chollet *et al.*, “Keras.” <https://github.com/keras-team/keras>, 2015.
- [46] J. Gallicchio, J. Huth, M. Kagan, M. D. Schwartz, K. Black, and B. Tweedie, “Multivariate discrimination and the Higgs + W/Z search,” *JHEP* **04** (2011) 069, [arXiv:1010.3698 \[hep-ph\]](#).